January 2016

An Automated Temporal, Amplitude, And Complexity-Based Comparison Of Commercial Plethysmographs

Matthew Mikhail
Yale University, matthew.mikhail@yale.edu

AN AUTOMATED TEMPORAL, AMPLITUDE, AND COMPLEXITY-BASED COMPARISON OF COMMERCIAL PLETHYSMOGRAPHS

A Thesis Submitted to the
Yale University School of Medicine
in Partial Fulfillment of the Requirements for the
Degree of Doctor of Medicine

by

Matthew Mikhail

2016

AN AUTOMATED TEMPORAL, AMPLITUDE, AND COMPLEXITY-BASED COMPARISON OF COMMERCIAL PLETHYSMOGRAPHS

Matthew Mikhail, Aymen Alian, and Kirk Shelley
Department of Anesthesiology, Yale University, School of Medicine, New Haven, CT.

The study of plethysmographic physiology has been limited by a lack of standardized and open plethysmographic hardware in clinical use. Fundamental differences in the processing of output between various devices obfuscate direct comparison, and the role played by physiology versus that by technology in the final viewable plethysmogram (PPG). This study proposes a largely automated, unbiased method for quantitatively comparing the outputs from proprietary pulse oximeter devices along three metrics: temporal delay, amplification, and complexity. It then applies these methods to the deconstruction of Masimo and Nellcor pulse oximeters.

With IRB approval, twelve healthy, awake subjects were studied. Each individual was attached simultaneously to a Nellcor ear probe and a Masimo finger device, and then instructed to perform incentive spirometry, Valsalva, and Mueller breathing maneuvers interspersed with normal breathing. For temporal delay and amplitude comparisons, the raw PPG data were first synchronized, then subsequently filtered into corresponding autonomic, respiratory, and cardiac frequency ranges. To assess the temporal delay, they were processed according to a sliding-window cross-correlation function, and the time shift of maximum correlation for each window was averaged, to determine a representative overall delay for each frequency range. For the amplitude analysis, the absolute value of the filtered data were integrated over a pre-determined time frame chosen at each frequency range, then divided to arrive at a ratio. These data were manually filtered to remove sequences corresponding to the noise artifact. Lastly, to assess pulse complexity, the raw data were converted from time-domain to frequency domain using digital Fast Fourier Transformation (dFFT), and an algorithm programmed to search for fundamental cardiac frequency, as well as the first five harmonic peaks. The dFFTs were then normalized

according to fundamental frequency peak, and the ratios of the amplitude of each harmonic peak to the corresponding harmonic peak from the other device were generated.

As outlined in the table below, the Nellcor device temporally led the Masimo in the respiratory and autonomic frequency ranges. Similarly, the Nellcor device demonstrated greater amplitude representation in those ranges as well. With regards to pulse complexity, however, the Masimo signal was better represented up to the first three harmonics. While the generalization of these results may be limited by the device placement, this study successfully presents a systematic method for comparing commercial hardware devices, paving the way for better understanding of this non-invasive modality.

Table 1. Overview of results, categorized by study metric.

	Temporal Shift	Amplification	Pulse Complexity
Masimo			**Greater detail** 1st Harmonic (p=0.0023) 2nd Harmonic (p=0.0003) 3rd Harmonic (p=0.0032)
Nellcor	**Leads** Respiratory - 0.37s (p= 0.0338) Autonomic – 0.72s (p=0.0024)	**Greater Representation** Respiratory – 5.95x (p<0.001) Autonomic – 10.84x (p<0.001)	

Acknowledgements

I, first and foremost, want to thank Dr. Kirk Shelley for his unwavering support and mentorship throughout the research process. From designing a good question through to developing methods and presenting at scientific meetings, he has taught me lessons that I will carry through my career. Moreover, Dr. Shelley showed me the importance of mentorship, and of having a career role-model to guide professional development.

I would also like to thank Dr. Aymen Alian, whose insight into the nuances of clinical monitoring were inspiring, and whose perspective was instrumental to the success of the project.

Finally, I would like to thank the family, friends and past mentors without whom there's no way I would be here today.

TABLE OF CONTENTS

INTRODUCTION

A. Origins of Plethysmography

The basis for plethysmography dates back to at least the 19th century, with Italian physiologist Angelo Mosso, who encased an arm in a fluid-filled chamber, akin to a manometer (Figure 1), to measure changes in limb-volume as a function of time [1]. This provided early information on the peripheral pulse and cardiac rhythm. Subsequently, work performed by Alrick Hertzman in the 1930's, updated the method to utilize light, and painted a much more detailed picture of vascular pulsatility (Figure 2) [2].

Figure 1. Early schematic depiction of Angelo Mosso's whole arm plethysmography, one of the first documented variations.

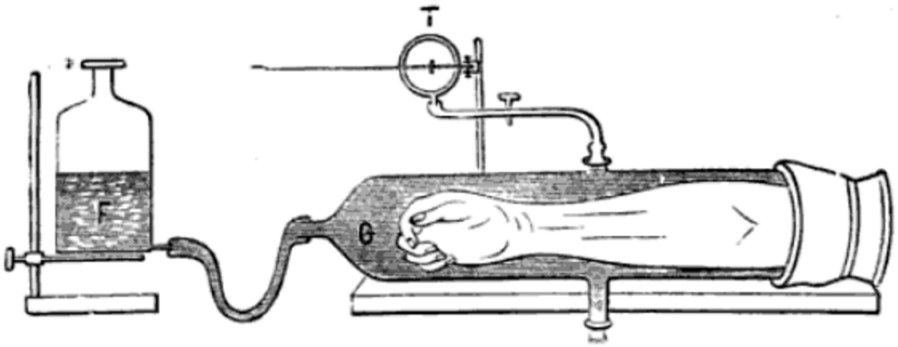

Mosso's plethysmograph. G, glass vessel for holding a limb; F, flask for varying the water pressure in G; T, recording apparatus.

Known in its entirety since 1851, the Beer-Lambert law governs the behavior of light as it passes through a non-scattering substance [3]. While this law gives a simplistic understanding that doesn't account for scattering within human tissue, it states that optical absorbance of light is directly proportional to the path-length traveled, as well as the concentration of absorbing molecules within it. It allows for optical transmission to act as a proxy of tissue diameter, and served as the basis for Hertzman's and all modern photoplethysmographic techniques. With the use of light also came the discovery that oxygenated and deoxygenated blood exhibit different optical absorbance characteristics, which paved the way for modern oximetry. Utilizing red and green wavelengths of light, Carl Matthes developed the first oxygen saturation meter device in 1935 [4]. This technology underwent multiple iterations, but remained largely bulky, impractical, and inaccurate until re-introduced by Nihon Kohden engineer Takuo Aoyogi in the 1970s. Aoyogi's technique isolated the absorbance information from the pulsatile component of the plethysmogram, thus eliminating artifact from bone and venous blood and greatly improving accuracy [5]. This technology entered the operating room setting and, within a decade, became the standard of care within all anesthetic settings.

Figure 2. Cardiac pulsations recorded from the finger pad, traced from Alrick Hertzman's early photoplethysmograph.

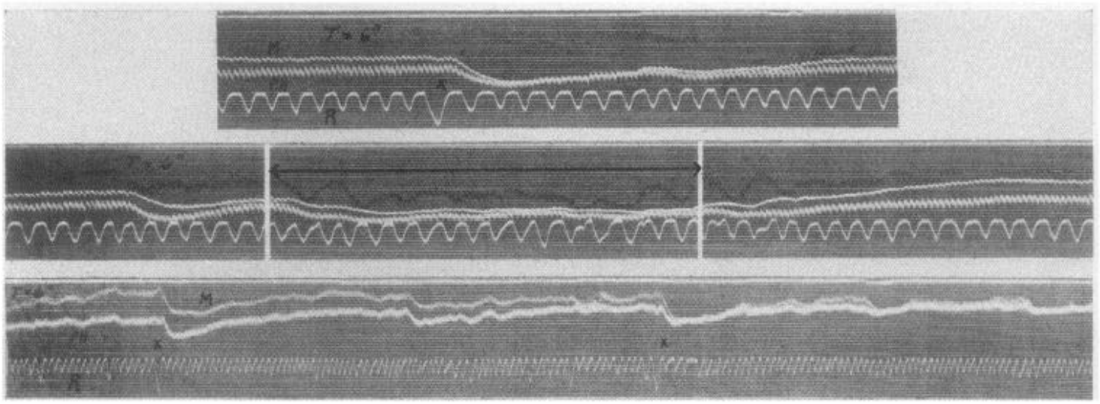

B. Current Understanding of PPG Physiology

While the initial understanding of the Beer-Lambert law guides photoplethysmograph implementation, numerous assumptions have been made to simplify the physics involved. At the more fundamental level is the assumption that the transmission medium is absorbing, but non-scattering. Anyone who's seen a finger-attached pulse oximeter can attest, however, that the entire digit glows with refracted and scattered light from the LED. This requires more complex physics and mathematics to understand [6]. Furthermore, within the heterogeneous finger, there is bone, blood, connective tissue, and numerous other components, each of which has its own light absorption characteristics. What this means from the oximetric perspective, is that

empirical algorithms have been required to calibrate saturations using volunteer reference subjects undergoing controlled arterial desaturation, and that no system for absolute calibration has been attainable [7].

Assuming a more complete understanding of those elements, however, there remains the question of path-length. While it's well-observed that the caliber of a finger varies with the cardiac cycle, it is yet unclear what causes this variation. What is clear is that vascular compliance contributes to this phenomenon, however the relative contribution of various levels of the vascular system is unclear [8]. There is evidence that arteriolar vessels dampen much of the blood's pulsatility into a smooth flow, and thus may be the level of the greatest volume change [9]. If so, this means oximeters more directly represent the arteriolar oxygen saturation, rather than the arterial content that is conventionally used as a proxy.

C. Deconstruction of the Photoplethysmographic Signal

Distinct physiological information can be isolated from different components of the raw PPG signal. When analyzed from the perspective of time-scale, it has been shown that the PPG can be deconstructed into at least four different physiologically relevant components. The first, traditionally represented, is cardiac information. This is localized to the the time-scales approaching the human pulse and may be fully encompassed within a frequency range of 0.5-2.0 Hz (30-120bpm). This information has proven useful in the monitoring of cardiac rhythm and heart rate variability, however it

lacks the subtler cardiovascular information within the contour of the cardiac pulse. Contour information can be isolated at frequencies greater than 2 Hz, and contains phenomena such as the incisura, or dicrotic notch, which is hypothesized to relate to factors including vascular compliance and distance from the aortic valve [10].

On the other end, longer time-scales can capture slower physiological phenomena, such as respiratory or autonomic influences on the vascular caliber and flow. At frequencies of 0.15-0.5 Hz (9-30 breaths/min), shifts in the venous blood associated with the respiratory cycle have been described.

Lastly, autonomic vascular changes are apparent at frequencies less than 0.15 Hz [11] and have the potential to convey anesthetic depth information and vascular sympathetic status.

D. Modern Landscape of Pulse Oximetry

With the advent of modern pulse oximetry came the industrial competition which saw a small number of manufacturers dominate the commercial market. Within the United States, Biox was the first commercial manufacturer of pulse oximetry technologies, however it saw its market share decline with the arrival of companies such as Nellcor and Masimo [5]. Since the fundamental basis for pulse oximetry was public domain, the edge was gained through the proprietary use of filters and signal processing in order to output more visually desirable plethysmograms (PPGs), and effectively function in the presence of mechanical,

electrical, or optical disruption. While this improved overall performance, it triggered debate as to the place of "black-box" devices within medical use [12]. Since the physiology underlying photoplethysmography is still not well-understood, these additional layers of abstraction act to further complicate PPG physiology research.

HYPOTHESIS

It is hypothesized that systematic analysis of the frequency subcomponents of two commercial pulse oximeters (Massimo and Nellcor) will allow for the development of an algorithm and transformative equations for conversion amongst them.

SPECIFIC AIMS

1. To develop a systematic method for synchronizing simultaneously gathered plethysmographic waveforms.
2. To develop a means of systematically deconstructing plethysmographic waveforms into frequency sub-components, performing operations on these components, and automating the comparison of these sub-components.
3. To devise a standard method for quantifying the degree of correlation between two plethysmographic waveforms.

METHODS

A. Data Collection

(Performed by Dr. Kirk Shelley and Dr. Aymen Alian)

With IRB approval, twelve healthy, awake volunteers were attached to multiple clinical monitors, including a Masimo Finger oximeter, a Nellcor Ear oximeter, and an inline airway pressure monitor. Each oximeter, along with the one shared airway pressure monitor, was attached to a separate data acquisition device, each recording at 100 Hz.

While attached to the devices, each subject was instructed to alternate between four activities: normal breathing, the Valsalva maneuver (exhalation against closed glottis), incentive spirometry, and Mueller breathing (inspiration against closed glottis). Recording times for each patient ranged from 15-25 minutes, and were saved for later processing.

B. Data Synchronization

(Performed by Matthew Mikhail)

The first step in signal analysis consisted of the synchronization of the PPG waveforms originating from separate data acquisition devices. Since each of the devices shared the same airway pressure, this pressure waveform was first used as a landmark for rough, manual synchronization (Figure 3).

Figure 3. a) Example of pre-synchronization airway pressure and PPG waveforms.
b) Waveforms following rough synchronization with airway pressure as the landmark.

a) b)

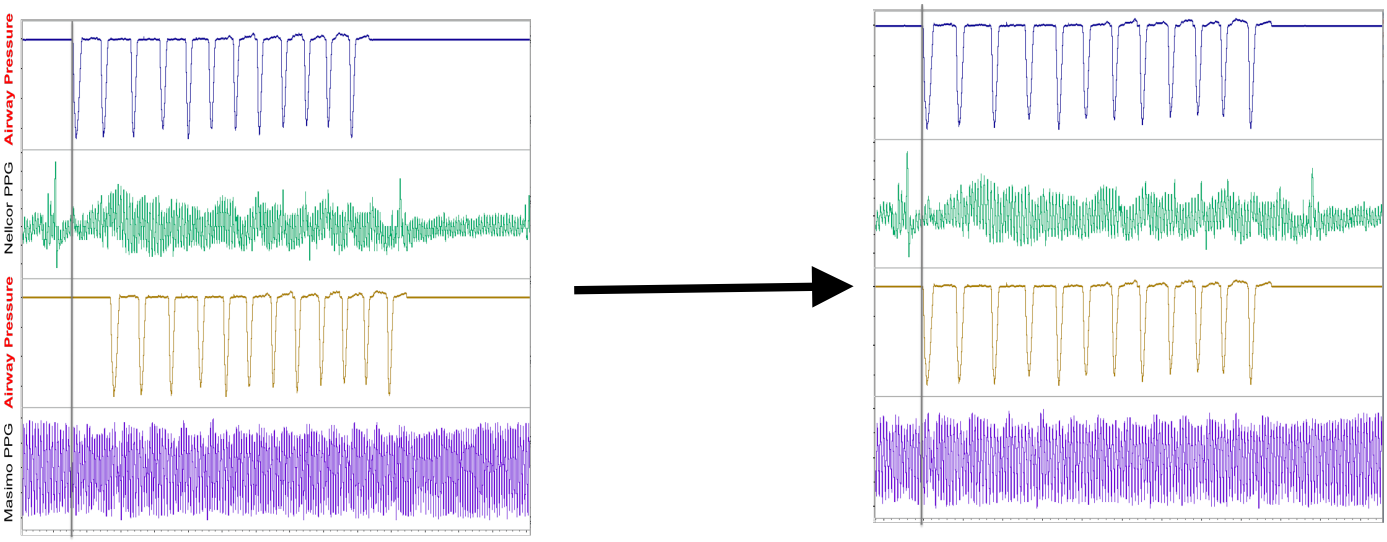

From there, more fine-tuned synchronization was performed through the use of automated digital cross-correlation of the full-length PPG waveforms against each other, identifying the time-shift associated with the maximum correlation between them, and then translating them by that amount (Figure 4).

$$(f * g)(\tau) = \int_{-\infty}^{\infty} f(t)g(t+\tau)dt$$

Figure 4. a) Schematic depiction of the cross-correlation function.

b) Plot of the resultant cross-correlation waveform, with peak representing time offset of the maximum agreement.

c) Pre- and post-synchronized PPG waveforms, using offset obtained from the correlation shown in b.

a)

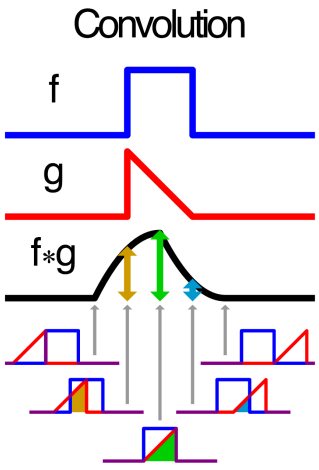

b)

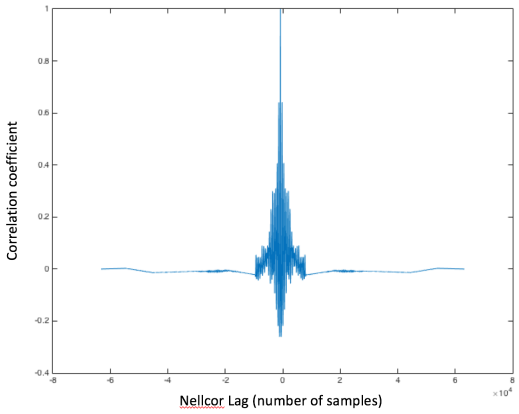

c)

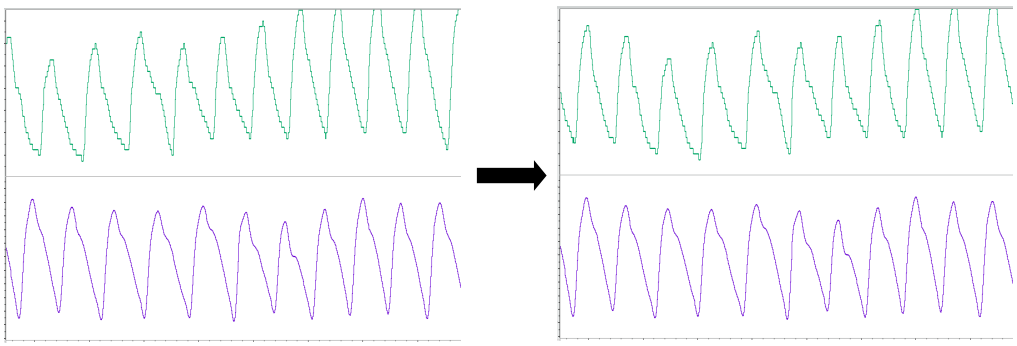

C. Data Analysis

(Performed by Matthew Mikhail)

Following overall synchronization, waveforms were analyzed according to three metrics: Temporal Shift, Scaling, and Complexity (Figure 5).

Figure 5. Visual depiction of the metrics of analysis.

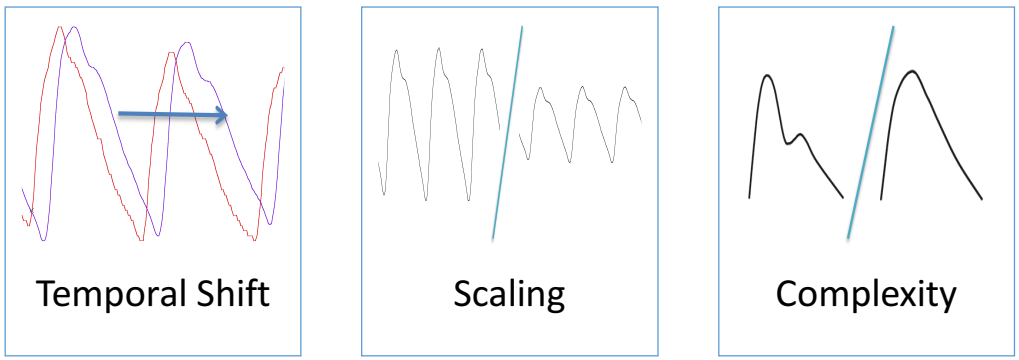

1. Temporal Shift Analysis

Given the hardware and software processing within commercial oximeters, it is hypothesized that frequency dependent time-shifts are introduced. As a result, band-pass filters were employed to deconstruct the signal into three physiologically relevant frequency ranges, and relative time-shift between the Nellcor and Masimo signals was evaluated independently for each. These time-ranges include cardiac (0.5-2.0 Hz), respiratory (0.15-0.5 Hz), and autonomic (0.01-0.15Hz) as previously outlined.

In order to overcome the effect of signal artifact on the synchronization of each frequency range, the component waveforms were cross-correlated in a stepwise fashion, using thirty second windows, advanced 1.5s per step (Figure 6). The time-offset of maximum agreement, as determined by cross-correlation, was obtained independently for each fragment, at each frequency range, then subsequently plotted against the fragment number for each waveform (Figure 7).

Figure 6. Illustration of data windows used for step-wise cross-correlation.

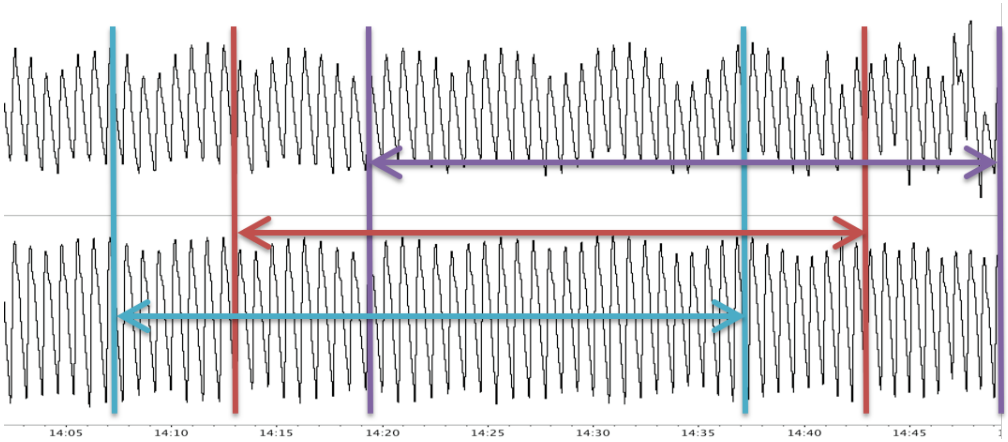

Figure 7. Time-delay of maximum correlation, plotted against the fragment number for each physiological frequency range.

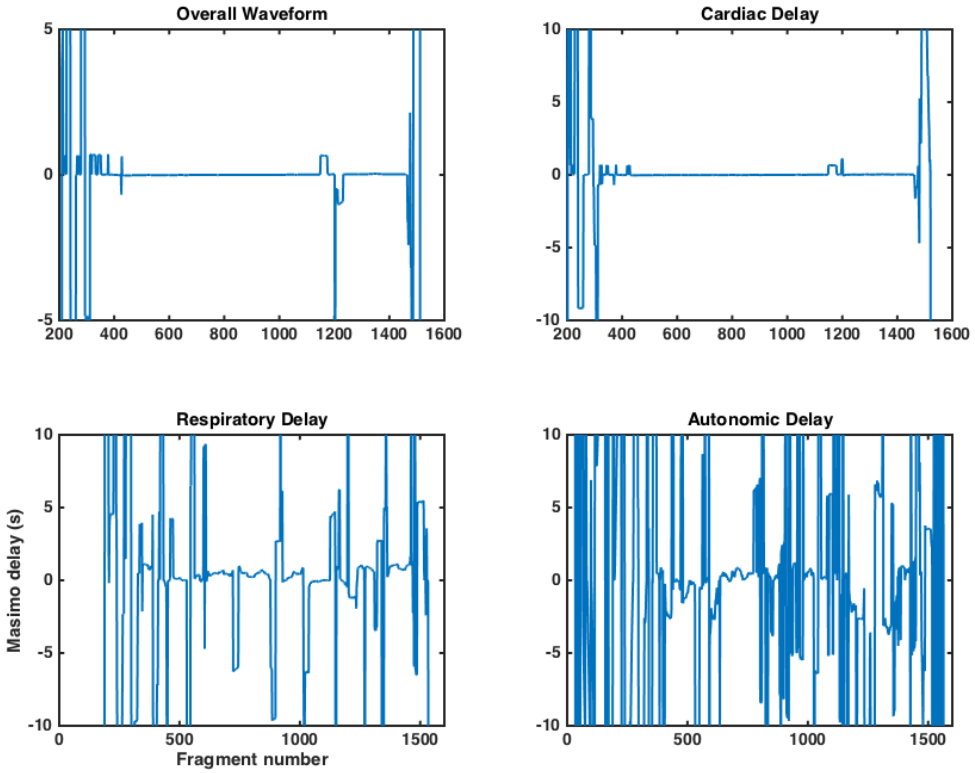

Subsequently, it was assumed that the large spikes from the fragment analysis plots represent spurious delays, and demonstrate a weaker correlation. This weak correlation was corroborated when the data were re-plotted by representing the value of the maximum correlation coefficient for each fragment by the color of the plotted point (Figure 8). Based on this, a correlation cutoff value of 0.8 was chosen as the point below

which data would be excluded. The remainder of the data points, those lying above this cutoff, were averaged to arrive at a final time-shift.

Figure 8. a) Example of the windowed cross-correlation of a single subject at respiratory frequency, with color denoting correlation coefficient (blue=low, orange=high).
b) Numeric depiction of the correlation coefficients.

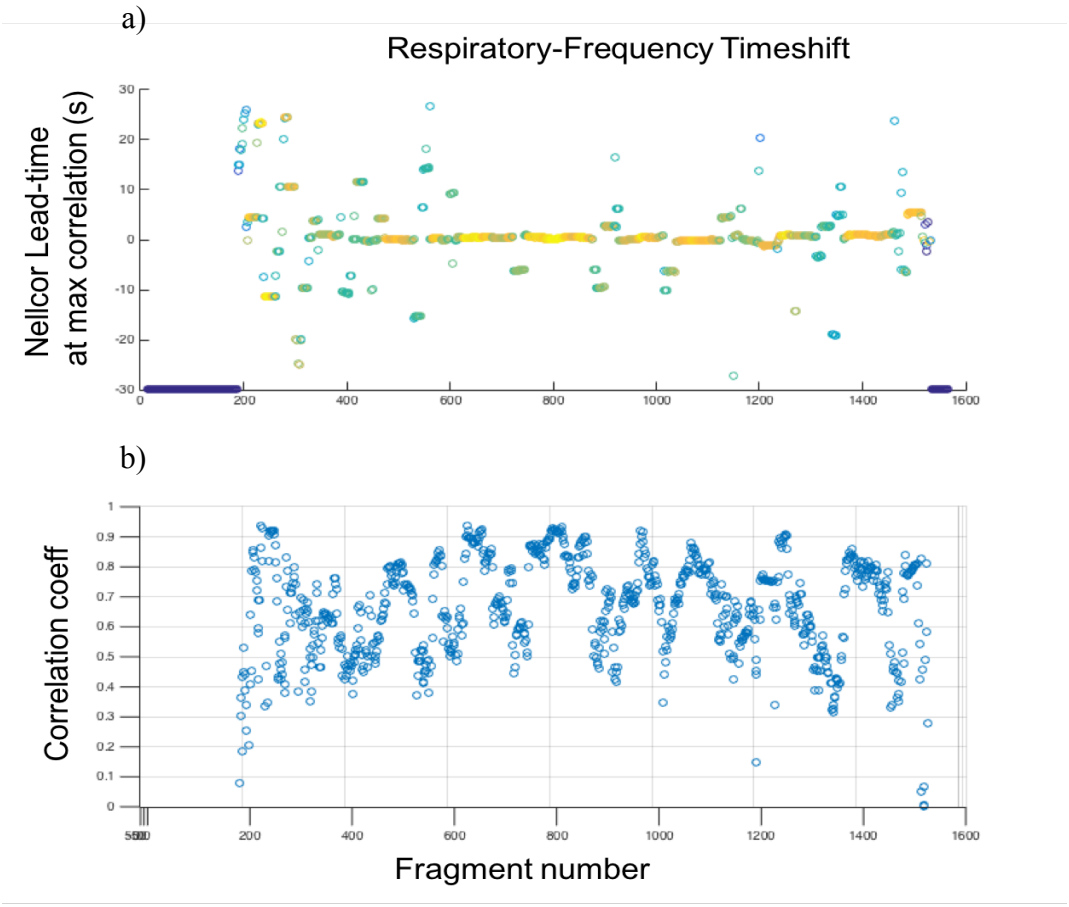

2. Scaling Analysis

For this component, the band-pass filtered PPG signals were used again. To better understand the relative amplification of the Nellcor and Masimo signals at

different physiological frequency ranges, each component-frequency signal was integrated over an arbitrarily chosen time period corresponding to approximately five physiological cycles of information. This equated to ~5 heart beats for the cardiac frequency (10s), ~5 breaths for the respiratory frequency (50s), and ~5 cycles for the autonomic vascular tone changes (100s).

For each window of integration, an amplitude ratio was calculated (Figure 9). The Nellcor/Masimo ratio of the integrated waveforms were then manually filtered to remove visible noise artifact, and the ratios of the amplitude for each time segment were averaged over the entirety of the sample length to arrive at a ratio that represents the relative amplitude of the Nellcor/Masimo signals for each subject.

Figure 9. Example of 10s timed-reset integral for cardiac PPGs.

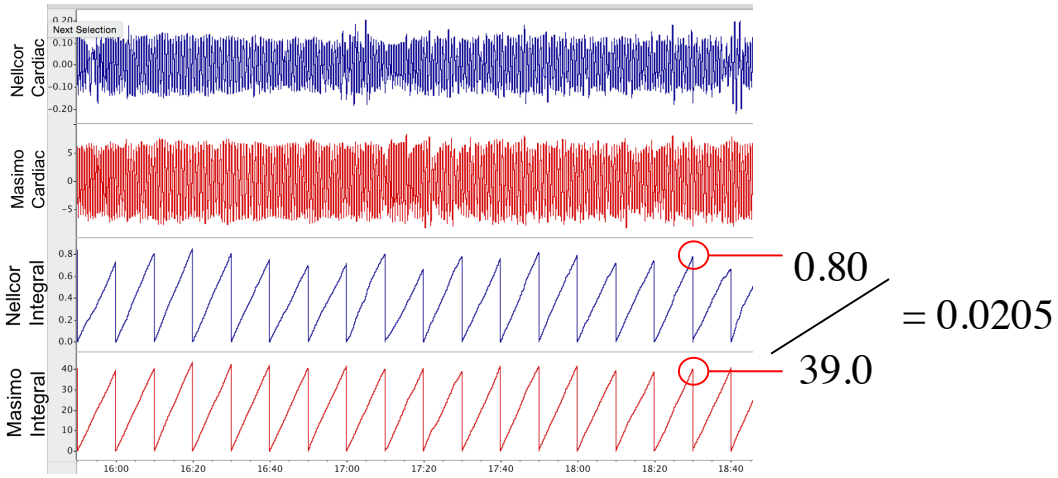

3. Complexity Analysis

The signal complexity comparison of the two oximeters was performed within the frequency domain as a means to preserve higher frequency, periodic data. The full-length raw PPG data were first divided into 20s fragments for each subject. Digital Fast Fourier Transformation was then performed on the raw Nellcor and Masimo fragments, utilizing a Hamming window, with FFT size of 2048 bins, and an amplitude spectral mode of analysis.

An algorithm was then devised and tested to search for and identify the fundamental cardiac frequency peak, along with the first five cardiac harmonics (Figure 10). The amplitude spectral density graphs were subsequently normalized to the fundamental cardiac peak amplitude and the ratio of the Masimo/Nellcor harmonic amplitude was determined. Finally, the ratios were averaged across all the fragments for a given subject, then across all the subjects to arrive at a relative measure of representation of the harmonic complexity.

Figure 10. Example of the dFFT representation of PPG, including first five harmonics, with sample calculation of the first harmonic.

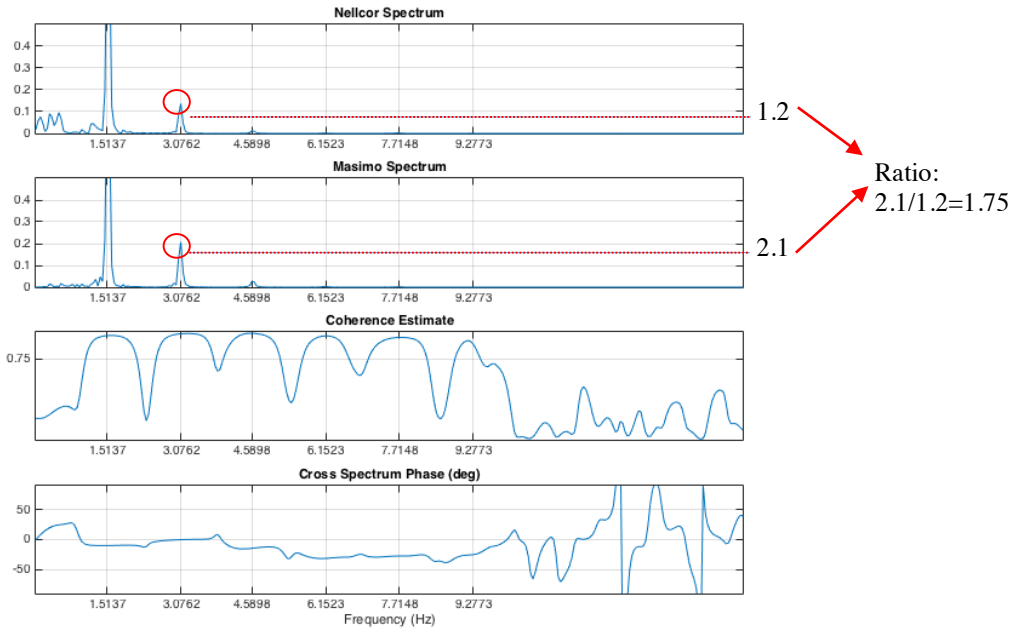

RESULTS

1. Temporal Shift Analysis

Using two-tailed student-t test to evaluate the difference between the Masimo and Nellcor devices with regard to time-delay, it was revealed that the Nellcor signal led the Masimo signal by 0.37s (p=0.0338) and 0.72s (p=0.0024), for the respiratory and autonomic ranges, respectively (Figure 11).

Figure 11. a) Nellcor signal lead-time, broken down by frequency range and individual subject. b) Average Nellcor signal lead-time.

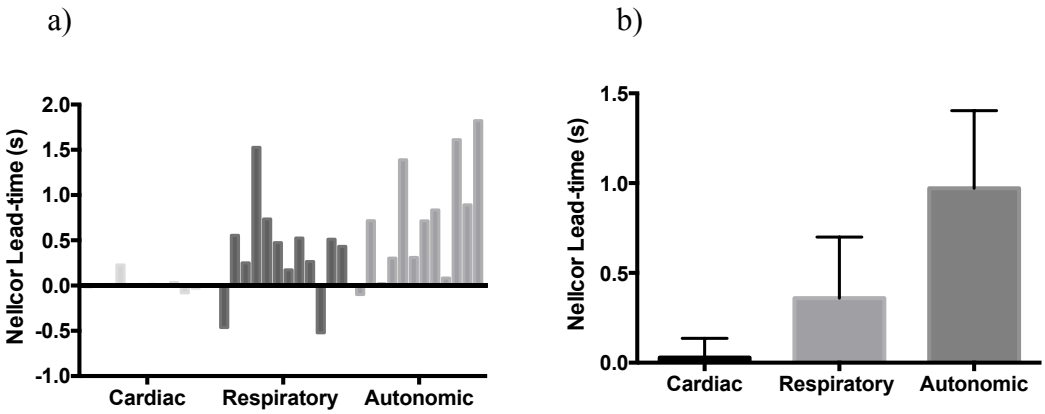

2. Scaling Analysis

Relative to the cardiac frequency range, the preservation of the respiratory and autonomic signals was greater in the Nellcor device than in the Masimo device, with Nellcor/Masimo signal ratios for respiratory and autonomic signals of 5.95-fold ($p<0.001$) and 10.48-fold ($p<0.001$), respectively (Figure 12).

Figure 12. a) Nellcor/Masimo signal scaling ratio, broken down by the frequency range and individual subject.
b) Average Nellcor/Masimo signal scaling ratio.

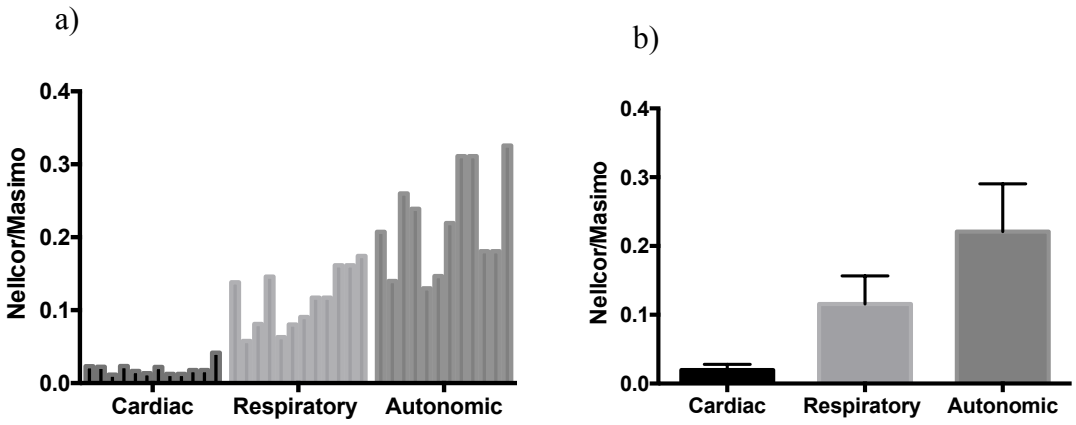

3. Complexity Analysis

Frequency domain analysis, averaged across all the subjects, demonstrated that the Masimo device preserved a greater degree of signal complexity than the Nellcor device, with statistically greater fidelity within the first three harmonics ($p=0.0023$, $p=0.0003$, and $p=0.0032$) as shown in Figure 13.

Figure 13. Masimo/Nellcor Harmonic Amplitude ratio, as averaged across all subjects for the first five harmonics.

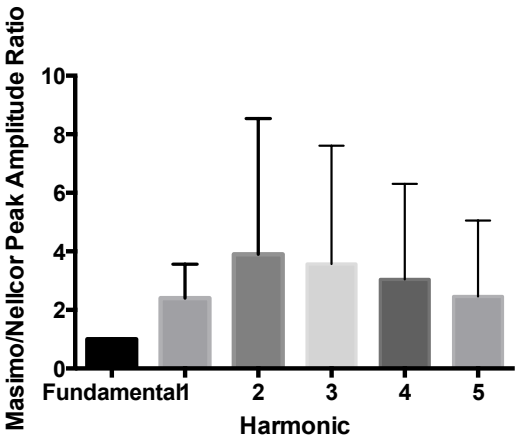

DISCUSSION

The future understanding of photoplethysmography rests on the ability to reliably interpret the PPG waveforms collected during real surgical settings, when human organ systems are stressed. A commonly acknowledged, but previously uninvestigated barrier to PPG research has been the proprietary, "black-box" nature of the instruments approved and widely employed to monitor this vascular physiology. While this study is not without limitations, it serves as a first effort to quantify these differences, and presents a systematic method for comparing proprietary devices on three metrics of clinical utility.

As a proof of method, however, there exist some fundamental limitations to the study design chosen. The choice to compare PPG readings from different bodily sites,

with Nellcor from an ear probe and Masimo from a finger probe, clouds direct brand comparison. What this study does, however, is reproduce previously documented phenomena, including increased respiratory variation of ear PPGs as compared to finger PPGs [13]. The more central location of ear vasculature may account for some of the observed lead-time in that device. Additionally, since the finger is peripheral and vasomodulates to a greater degree based on sympathetic tone, there may be a greater likelihood that the subtle systemic autonomic blood fluctuations would be dampened in the finger, thus accounting for the lowered autonomic representation.

This study also provides powerful tools for future plethysmographic research. Rather than being used as a barometer for performance of various plethysmographs, it is hoped that a more complete understanding of the trade-offs that go into the signal-processing for these oximeters can inform their design. Ideally, future studies would be able to take this work in one of two interesting directions. The first is to obtain head-to-head comparisons of different devices placed on the same appendage, which would allow for an isolated comparison of the technological differences at play. The second approach is to analyze the same device on different appendages, and thus further explore the physiologic differences in PPG signal that reaches various locations in the body. By expanding these realms of knowledge, the ultimate hope is that this will allow clinicians to use the tools readily available to make more informed decisions regarding the care of their patients.

REFERENCES

1. Landois, L., *Textbook of human physiology*. 1889.
2. Hertzman, A.B., *The blood supply of various skin areas as estimated by the photoelectric plethysmograph.* Am. J. Physiol., 1938. **124**(2): p. 328-340.
3. August, B., *Versuch der absorptions-verhaltnisse des cordierites fur rothes licht zu bestimmen.* Ann Physik Chem (German), 1851. **84**: p. 37-52.
4. Severinghaus, J.W. and P.B. Astrup, *History of blood gas analysis. VI. Oximetry.* Journal of Clinical Monitoring, 1986. **2**(4): p. 270-88.
5. Severinghaus, J. and Y. Honda, *History of blood gas analysis. VII. Pulse oximetry.* Journal of Clinical Monitoring, 1987. **3**(2): p. 135-138.
6. Mannheimer, P.D., *The Light Tissue Interaction of Pulse Oximetry.* Anesth Analg, 2007. **105**(6S_Suppl): p. S10-17.
7. Alian, A.A. and K.H. Shelley, *Photoplethysmography.* Best Pract Res Clin Anaesthesiol, 2014. **28**(4): p. 395-406.
8. Kim, J.M., et al., *Pulse oximetry and circulatory kinetics associated with pulse volume amplitude measured by photoelectric plethysmography.* Anesth Analg, 1986. **65**(12): p. 1333-9.
9. Spigulis, J., *Optical noninvasive monitoring of skin blood pulsations.* Appl Opt, 2005. **44**(10): p. 1850-7.
10. Murray, W.B. and P.A. Foster, *The peripheral pulse wave: information overlooked.* J Clin Monit, 1996. **12**(5): p. 365-77.

11. Galante, N.G., et al. *The Ear PPG Oscillates at the 0.12-0.18 Hz Autonomic Frequency during Lower Body Negative Pressure.* . in *ASA Annual Meeting*. 2008.

12. Ruskin, K.J. and K.H. Shelley, *Patent Medicine and The "Black Box".* Anesth Analg, 2005. **100**(5): p. 1361-1362.

13. Clayton, D.G., et al., *Pulse oximeter probes. A comparison between finger, nose, ear and forehead probes under conditions of poor perfusion.* Anaesthesia, 1991. **46**(4): p. 260-5.

APPENDIX

A. Windowed, threshold cross-correlation function Script

```
function [ shiftAve,shiftSD ] =
WindowedCorrThresholdFn(file,fraglength,overlap,threshold)
%UNTITLED3 Summary of this function goes here
%   Detailed explanation goes here

    load(file)

    if ~exist('data','var'),
        error('No data! Select a mat file that contains data and was created with Export
Matlab 3.0 or later (LabChart for Windows 7.2 or later)')
        return
    end

    [numchannels, numblocks] = size(datastart);
    [~,length] = size(data);
    length=length/numchannels;

    overlap = overlap/100;

    fraglengthSamples=fraglength*100;

    numfrags=floor((length-fraglengthSamples)/(fraglengthSamples*(1-overlap))+1);

    pdatarray = zeros(numchannels,length);
    xcorrarray = zeros (numchannels,numchannels,2*length-1);
    xcorrlagarray = zeros (numchannels,numchannels,2*length-1);
    fragXcorrArray = zeros (numchannels,numchannels,numfrags,2*fraglengthSamples-1);
    fragXcorrLagArray = zeros (numchannels,numchannels,numfrags,2*fraglengthSamples-1);
    I = zeros (numchannels,numchannels);
    fragI = zeros (numchannels,numchannels,numfrags);
    corrval = zeros (numchannels,numchannels);
    fragcorrval = zeros (numchannels, numchannels, numfrags);
    t = zeros (numchannels,numchannels);
    fragT= zeros (numchannels,numchannels,numfrags);

    nellcor=1;
    masimo=2;
    n_card=3;
    m_card=6;
    n_resp=4;
    m_resp=7;
    n_auto=5;
    m_auto=8;

    fragdatarray=zeros(numchannels,numfrags,fraglengthSamples);
```

```
    for ch = 1:numchannels,
        pdatarray(ch,:) = data(datastart(ch,1):dataend(ch,1));
    end

    for ch = 1:numchannels,
        for curfrag=1:numfrags
            fragdatarray(ch,curfrag,:) = pdatarray(ch,(floor((curfrag-1)*(1-
overlap)*(fraglengthSamples))+1):(floor((curfrag-1)*(1-
overlap)*(fraglengthSamples))+fraglengthSamples));
        end
    end

    for ch2 = 1:numchannels,
        for ch1 = 1:ch2,
            for curfrag=1:numfrags

[fragXcorrArray(ch1,ch2,curfrag,:),fragXcorrLagArray(ch1,ch2,curfrag,:)] =
xcov(fragdatarray(ch1,curfrag,:),fragdatarray(ch2,curfrag,:),'coeff');
                  [fragcorrval(ch1,ch2,curfrag),fragI(ch1,ch2,curfrag)] =
max(fragXcorrArray(ch1,ch2,curfrag,:));
                  fragT(ch1,ch2,curfrag) =
fragXcorrLagArray(ch1,ch2,curfrag,fragI(ch1,ch2,curfrag));
            end
        end
    end

    fragTsec = fragT/100;

    fragTthresh=fragTsec;
    fragCorrValThresh=fragcorrval;

    for ch2=1:numchannels
        for ch1=1:ch2
            for curfrag=1:numfrags
                if (fragCorrValThresh(ch1,ch2,curfrag)>=threshold) &&
(abs(fragTthresh(ch1,ch2,curfrag))<4)
                else
                    fragCorrValThresh(ch1,ch2,curfrag)=NaN;
                    fragTthresh(ch1,ch2,curfrag)=NaN;
                end
            end
        end
    end

    cardAve = nanmean(squeeze(fragTthresh(3,6,:)));
    respAve = nanmean(squeeze(fragTthresh(4,7,:)));
    autoAve = nanmean(squeeze(fragTthresh(5,8,:)));

    cardSD = nanstd(squeeze(fragTthresh(3,6,:)));
```

```
    respSD = nanstd(squeeze(fragTthresh(4,7,:)));
    autoSD = nanstd(squeeze(fragTthresh(5,8,:)));

    shiftAve=[cardAve respAve autoAve];
    shiftSD=[cardSD respSD autoSD];


end
```

B. Harmonic Peak-Finding algorithm

```
function [ratioAve,ratioSD] = HarmonicRatioFn(file,fraglength,overlap)
%UNTITLED3 Summary of this function goes here
%   Detailed explanation goes here

load(file)

if ~exist('data','var'),
    error('No data! Select a mat file that contains data and was created with Export
Matlab 3.0 or later (LabChart for Windows 7.2 or later)')
    return
end

[numchannels, numblocks] = size(datastart);
[~,length] = size(data);
length=length/numchannels;

overlap = overlap/100;
nfft=2048;

fraglengthSamples=fraglength*100;

numfrags=floor((length-fraglengthSamples)/(fraglengthSamples*(1-overlap))+1);

pdatarray = zeros(2,length);
fragCohereArray = zeros (numfrags,floor((nfft/2 + 1)));
fragCohereLagArray = zeros (numfrags,floor((nfft/2 + 1)));
fragPeriodArray = zeros (2,numfrags,floor((nfft/2 + 1)));
fragPeriodLagArray = zeros (2,numfrags,floor((nfft/2 + 1)));
Pxy=zeros (numfrags,floor((nfft/2 + 1)));
pks = zeros(3,numfrags,6);
locs = zeros(3,numfrags,6);
harmonic_ratio = zeros(numfrags,6);
fundPos = zeros(2,numfrags);
fundHeight = zeros(2,numfrags);


nellcor=1;
masimo=2;
```

```
fragdatarray=zeros(2,numfrags,fraglengthSamples);


for ch = 1:2,
        pdatarray(ch,:) = data(datastart(ch,1):dataend(ch,1));
end

for ch = 1:2,
    for curfrag=1:numfrags
        fragdatarray(ch,curfrag,:) = pdatarray(ch,(floor((curfrag-1)*(1-
overlap)*(fraglengthSamples))+1):(floor((curfrag-1)*(1-
overlap)*(fraglengthSamples))+fraglengthSamples));
    end
end


for curfrag=1:numfrags
            [fragPeriodArray(1,curfrag,:),fragPeriodLagArray(1,curfrag,:)]
=periodogram(squeeze(fragdatarray(1,curfrag,:)),hamming(fraglengthSamples,'periodic'),nff
t,100,'psd');
            [fragPeriodArray(2,curfrag,:),fragPeriodLagArray(2,curfrag,:)]
=periodogram(squeeze(fragdatarray(2,curfrag,:)),hamming(fraglengthSamples,'periodic'),nff
t,100,'psd');

            fragPeriodArray(1,curfrag,:)=sqrt(fragPeriodArray(1,curfrag,:));
            fragPeriodArray(2,curfrag,:)=sqrt(fragPeriodArray(2,curfrag,:));

            [fundHeight(1,curfrag),fundPos(1,curfrag)]=max(fragPeriodArray(1,curfrag,:));
            [fundHeight(2,curfrag),fundPos(2,curfrag)]=max(fragPeriodArray(2,curfrag,:));

            if abs(fundPos(2,curfrag)-fundPos(1,curfrag))>5
                if fundPos(2,curfrag)>3

[fundHeight(1,curfrag),fundPos(1,curfrag)]=max(fragPeriodArray(1,curfrag,fundPos(2,curfra
g)-3:fundPos(2,curfrag)+3));
                    fundPos(1,curfrag)=fundPos(1,curfrag)+fundPos(2,curfrag)-4;
                elseif fundPos(1,curfrag)>3

[fundHeight(2,curfrag),fundPos(2,curfrag)]=max(fragPeriodArray(2,curfrag,fundPos(1,curfra
g)-3:fundPos(1,curfrag)+3));
                    fundPos(2,curfrag)=fundPos(2,curfrag)+fundPos(1,curfrag)-4;
                end
            end


fragPeriodArray(1,curfrag,:)=fragPeriodArray(1,curfrag,:)/fundHeight(1,curfrag);

fragPeriodArray(2,curfrag,:)=fragPeriodArray(2,curfrag,:)/fundHeight(2,curfrag);

            minDist1=max([floor(0.9*fundPos(1,curfrag)) 10]);
```

```
            minDist2=max([floor(0.9*fundPos(2,curfrag)) 10]);

            [fragCohereArray(curfrag,:),fragCohereLagArray(curfrag,:)] =
mscohere(squeeze(fragdatarray(1,curfrag,:)),squeeze(fragdatarray(2,curfrag,:)),[],[],nfft
,100);

Pxy(curfrag,:)=cpsd(squeeze(fragdatarray(1,curfrag,:)),squeeze(fragdatarray(2,curfrag,:))
,[],[],nfft,100);


  %          if
~isempty(findpeaks(squeeze(fragCohereArray(curfrag,minDist2:end)),'MinPeakDistance',minDi
st2,'Sortstr','descend','NPeaks',3))
   %             [pks(3,curfrag,:),locs(3,curfrag,:)] =
findpeaks(squeeze(fragCohereArray(curfrag,minDist2:end)),'MinPeakDistance',minDist2,'Sort
str','descend','NPeaks',3);
    %            locs(3,curfrag,:)=locs(3,curfrag,:)+minDist2-1;
     %       end

            if
~isempty(findpeaks(squeeze(fragPeriodArray(1,curfrag,minDist1:end)),'MinPeakDistance',min
Dist1,'Sortstr','descend','NPeaks',2)) &&
isequal(size(squeeze(findpeaks(squeeze(fragPeriodArray(1,curfrag,minDist1:end)),'MinPeakD
istance',10,'Sortstr','descend','NPeaks',2))),size(squeeze(pks(1,curfrag,1:2))))
                [pks(1,curfrag,1:2),locs(1,curfrag,1:2)] =
findpeaks(squeeze(fragPeriodArray(1,curfrag,minDist1:end)),'MinPeakDistance',minDist1,'So
rtstr','descend','NPeaks',2);
                locs(1,curfrag,1:2)=locs(1,curfrag,1:2)+minDist1-1;
                locMin=locs(1,curfrag,2)-locs(1,curfrag,1)-3;
                locMax=locs(1,curfrag,2)-locs(1,curfrag,1)+3;
                for i=3:6
                    j=i-1;
                    searchMin=locs(1,curfrag,j)+locMin;
                    searchMax=locs(1,curfrag,j)+locMax;
                    if searchMin>0 &&
searchMax<=max(size(squeeze(fragPeriodArray(1,curfrag,:)))) &&
~isempty(findpeaks(squeeze(fragPeriodArray(1,curfrag,searchMin:searchMax)),'Sortstr','des
cend','NPeaks',1))

[pks(1,curfrag,i),tempLoc]=findpeaks(squeeze(fragPeriodArray(1,curfrag,searchMin:searchMa
x)),'Sortstr','descend','NPeaks',1);
                        locs(1,curfrag,i)=searchMin+tempLoc-1;
                    end
                end
            end

            if
~isempty(findpeaks(squeeze(fragPeriodArray(2,curfrag,minDist2:end)),'MinPeakDistance',min
Dist2,'Sortstr','descend','NPeaks',2)) &&
```

```
isequal(size(squeeze(findpeaks(squeeze(fragPeriodArray(2,curfrag,minDist2:end)),'MinPeakD
istance',10,'Sortstr','descend','NPeaks',2))),size(squeeze(pks(2,curfrag,1:2))))
                [pks(2,curfrag,1:2),locs(2,curfrag,1:2)] =
findpeaks(squeeze(fragPeriodArray(2,curfrag,minDist2:end)),'MinPeakDistance',minDist2,'So
rtstr','descend','NPeaks',2);
                locs(2,curfrag,1:2)=locs(2,curfrag,1:2)+minDist2-1;
                locMin=locs(2,curfrag,2)-locs(2,curfrag,1)-3;
                locMax=locs(2,curfrag,2)-locs(2,curfrag,1)+3;
                for i=3:6
                    j=i-1;
                    searchMin=locs(2,curfrag,j)+locMin;
                    searchMax=locs(2,curfrag,j)+locMax;
                    if searchMin>0 &&
searchMax<=max(size(squeeze(fragPeriodArray(2,curfrag,:)))) &&
~isempty(findpeaks(squeeze(fragPeriodArray(2,curfrag,searchMin:searchMax)),'Sortstr','des
cend','NPeaks',1))

[pks(2,curfrag,i),tempLoc]=findpeaks(squeeze(fragPeriodArray(2,curfrag,searchMin:searchMa
x)),'Sortstr','descend','NPeaks',1);
                        locs(2,curfrag,i)=searchMin+tempLoc-1;
                    end
                end

                if
abs(fragPeriodArray(2,curfrag,locs(2,curfrag,1))/fragPeriodArray(1,curfrag,locs(2,curfrag
,1))-1)<0.15 && max(locs(2,curfrag,:))<(7*min(locs(2,curfrag,:))) &&
min(locs(2,curfrag,i))~=0 && min(locs(1,curfrag,i))~=0

harmonic_ratio(curfrag,:)=fragPeriodArray(2,curfrag,locs(2,curfrag,:))./fragPeriodArray(1
,curfrag,locs(2,curfrag,:));
                end
            end


end

        phase=-angle(Pxy)/pi*180;
        %Masimo/Nellcor ratio of amplitude of harmonics after fundamental
        %frequency normalized to amplitute 1
        harmonic_ratio_squeeze = harmonic_ratio(all(harmonic_ratio~=0,2),:);
        for i=1:6
            ratioAve(i)=nanmean(squeeze(harmonic_ratio_squeeze(:,i)));
            ratioSD(i)=nanstd(squeeze(harmonic_ratio_squeeze(:,i)));
        end
    ratioAve = squeeze(transpose(ratioAve))
    ratioSD = squeeze(transpose(ratioSD))
end
```